Supplementary Information

Mechanochemical processing of interface-integrated mixed-matrix membranes for efficient gas separations

Kunxiang Lei[1], Xinxi Huang[1], Yihao Xiao[1], Kun Niu[1], He Huang[2], Zhiwei Qiao[2]*, Wanbin Li[1]*

[1]College of Environment and Climate, Jinan University, Guangzhou 511443, China

[2]School of Chemistry and Chemical Engineering, Guangzhou University, Guangzhou, 510006, China

*Corresponding authors: gandeylin@126.com (W.L.); zqiao@gzhu.edu.cn (Z.Q.)

Methods

Materials

Zirconium tetrachloride ($ZrCl_4$, 98%, Aladdin), 2-aminobenzene-1,4-dicarboxylic acid (NH_2-BDC, 98%, Macklin), benzenedicarboxylic acid (BDC, 99%, Aladdin), *N*,*N*-dimethylformamide (DMF, 99.5%, Guanghua), chloroform (99%, Guangshi), dichloromethane (99.5%, Guanghua), potassium carbonate (K_2CO_3, 99%, Macklin), methanol (99.5%, Guanghua), toluene (99.5%, Guangshi), acetone, N-methyl-2-pyrrolidone (NMP, 99%, Macklin), ethanol (99.7%, Guanghua), 2,3,5,6-tetrafluoroterephthalonitrile (TFTPN, 99%, Macklin), 5,5',6,6'-tetrahydroxy-3,3,3',3'-tetramethyl-1,1'-spirobisindane (TTSBI, 96%, Aladdin) were purchased from Kutai Chemical Reagent Co. China and Sigma-Aldrich. K_2CO_3 was dried at 120 ^{o}C overnight before use. TTSBI was purified by crystallization in methanol and dichloromethane.

Synthesis of PIM-1

For synthesis of PIM-1, the TTSBI (0.01 mol), dried K_2CO_3 (0.03 mol), and TFTPN (0.01 mol) were dissolved in a mixture of NMP (20.0 mL) and toluene (10.0 mL). Polymerization reaction was carried out at 160 ^{o}C for 40 min under nitrogen atmosphere. After synthesis, the precipitated product was collected by adding methanol and centrifugation. For purification, the yellow product was dissolved in chloroform and re-precipitated in methanol, and then washed by deionized water and acetone for three times. Finally, the obtained PIM-1 was dried in vacuum at 100 ^{o}C for 48 h.

Solution-mixing fabrication of UiO_N@PIM MMMs

For solution-mixing fabrication, the UiO_N powder was dispersed in chloroform and the PIM-1 powder was added in chloroform to form a PIM-1 solution with concentration of 5.0 wt%.

Then, the PIM-1 solution was filtered into the UiO_N suspension using a polytetrafluoroethylene filter. After stirring overnight and sonication to remove air bubbles, the casting ink was poured into a Teflon dish and evaporated at room temperature for solidification and formation of MMM. Finally, the prepared membrane was soaked in methanol and dried at 100 ^{o}C. Similarly, the procedures for processing of UiO@PIM MMM were the same as those for UiO_N@PIM MMM, except replacing UiO_N by UiO.

Isolation of M_p-UiO_N and M_p-PIM

The UiO_N and PIM-1 powders were added in chloroform and transferred into a Teflon container with 4 or 5 agate balls to perform ball milling. After ball milling at 1200 rpm for 1 h by planetary ball milling, the casting ink were centrifuged to separate filler (M_p-UiO_N) and PIM-1 (M_p-PIM). The M_p-UiO_N was washed by $CHCl_3$ for over 20 times to remove physically adhesive PIM-1. After dried in 80 ^{o}C for 10 h, M_p-UiO_N powder was obtained. During separation, the supernatant PIM-1 was re-precipitated in methanol, and then washed by deionized water and acetone for three times to obtain M_p-PIM.

Characterizations

A field emission scanning electron microscopy (SEM, Ultra-55, Zeiss Co.) with voltage of 5 kV was used to observe the membrane morphologies. For capturing cross-sectional images, the membrane was fractured in liquid nitrogen. Before observation, the sample was coated with a thin layer of platinum. A transmission electron microscope (TEM, JEM-2100, JEOL Ltd.) with accelerating voltage of 200 kV was used to observe microstructures of samples. For sample preparation, the sample was dispersed in ethanol suspension, dropped onto a copper mesh-supported carbon film, and then dried at room temperature. Element distributions were measured through the attached x-ray energy dispersion spectroscope. An x-

ray diffractometer (XRD, D8, Advanced, Bruker Co.) with Cu Kα radiation and wavelength of 0.154056 nm was employed to investigate the crystalline structures of MMMs and MOFs. A physisorption analyzer (Autosorb iQ Station, Quantachrome Instruments) was sued to collect nitrogen adsorption-desorption isotherms at 77 K and gas sorption isotherms at 298 K. Multipoint Brunauer-Emmett-Teller method was used to quantify the specific surface areas of samples. Gas uptakes of MMMs were measured at 25 ^{o}C by using the same analyzer. Before measurement, the sample was cut into small pieces and thermally treated under vacuum condition at 120 ^{o}C for 16 h. A thermogravimetric analyzer (TGA, Q5000 V3.17 Build 265) with air purging and heating rate of 10 ^{o}C min^{-1} was employed to study the thermal stability of samples. A Fourier transform infrared spectroscope (FTIR, IRTracer-100, Shimadzu Co.) was used to evaluate chemical structures of samples. For membranes, the FTIR was operated with mode of attenuated total reflectance. An x-ray photoelectron spectrophotometer (XPS, K-Alpha, Thermo Fisher Scientific Inc., USA) was used to analyze the binding states of samples. A gel permeation chromatography (GPC, 1260 Infinity, Agilent Tech. Inc., USA) was used to measure the molecular weight (M_w) distributions of PIM-1 and M_p-PIM. Tetrahydrofuran was used as the solvent. Raman spectra of samples were collected using DXR 2xi (Thermo Fisher Scientific Inc., USA) with a 532 nm excitation laser. X-ray total scattering data were measured at the PD beamline at the Australian Synchrotron, using a Mythen II detector over 124° 2θ. Samples were packed into 0.7 mm borosilicate capillaries and rotated during data collection. The wavelength, zero error, and instrument contribution to the peak shape were refined to 0.5891(1) Å using NIST LaB6 660b. Energy was calibrated with NIST LaB6 standard. The simplified structure factor S(Q) was calculated using the scattering data. And the pair distribution function (PDF) in form of G(r) was obtained by Fourier transforming the scattering data. Q was the scattering vector whose magnitude was 4π

sin θ/λ, where 2θ was the scattering angle and λ was the incident radiation wavelength, 0.5905 Å. The PDF data were converted by PDFgetX3 software package.

Molecular dynamics (MD) simulation

The atoms in the bidentate, monodentate, and disconnected UiO_N and in the PIM-1 were described by the Lennard−Jones (LJ) and electrostatic potentials. The LJ potential parameters of Zr atom were adopted from the universal force field.[1] By fitting the electrostatic potentials, the atomic charges were using the M-QEq method.[2] The other atoms were described as charged LJ particles by the AMBER force field.[3] Initially, each simulation system was subjected to energy minimization using the steepest descent method with a maximum step size of 0.1 Å and a force tolerance of 1 kJ/(mol Å). Then, velocities were assigned according to the Maxwell−Boltzmann distribution. Finally, MD simulation was carried out at 25°C. Temperature was controlled by the velocityrescaled Berendsen thermostat with a relaxation time of 0.1 ps. The membrane was assumed to be flexible during simulation. A cutoff of 14 Å was used to calculate the LJ interactions, and the particle-mesh Ewald method was used to evaluate the electrostatic interactions with grid spacing of 1.2 Å and real-space cutoff of 14 Å. A time step of 2 fs was used to integrate the equations of motion by leapfrog algorithm, and the simulation duration was 8 ns.

Sorption-diffusion model

Sorption coefficient was calculated based on the CO_2, CH_4, and N_2 uptakes using Henry's law. Adsorption isotherms of MMMs were measured by using a dual-mode sorption model. CO_2, CH_4, and N_2 adsorption isotherms were fitted by the following equation:

$$C = K_d p + \frac{c'_h bp}{1 + bp} \tag{1}$$

Where C was concentration for adsorbed component. K_d were Henry's solubility and c'_h represented Langmuir equilibrium constants. p and b were adsorbate gas pressure at equilibrium and Langmuir affinity constant, respectively.

Sorption coefficient (S) was calculated using the following equation:

$$S = \frac{C}{p} = K_d + \frac{c'_h b}{1 + bp} \tag{2}$$

Diffusion coefficient (D) was calculated by:

$$D = \frac{P}{S} \tag{3}$$

Sorption selectivity was expressed as follows:

$$Sorption\ selectivity = \frac{S_A}{S_B} \tag{4}$$

Where S_A and S_B were sorption coefficients of A and B, respectively.

Diffusion selectivity was expressed as follows:

$$Diffusion\ selectivity = \frac{D_A}{D_B} \tag{5}$$

Where D_A and D_B were diffusion coefficients of A and B, respectively.

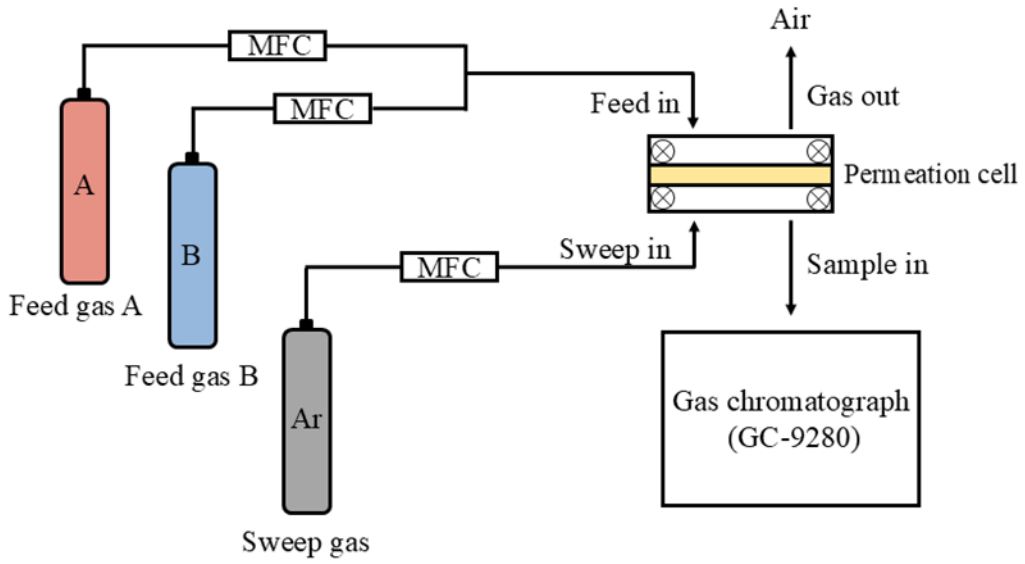

Fig. S1. Schematic diagram of self-made apparatus for gas separation. MFC: mass flow controller.

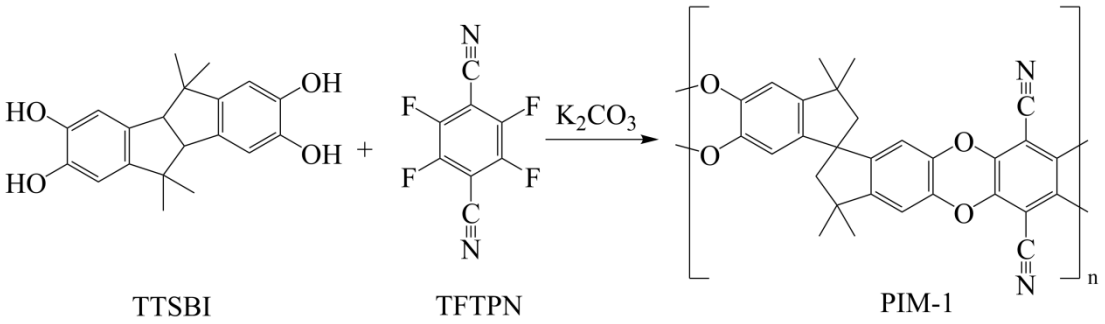

Fig. S2. Synthesis of PIM-1.

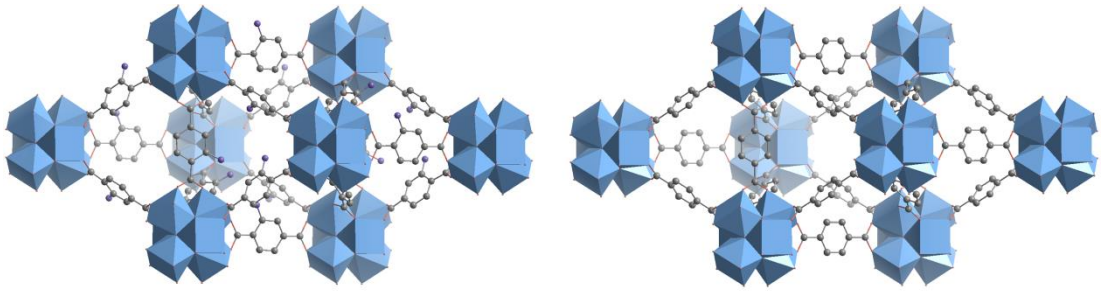

Fig. S3. Cubic units of UiO-66-NH_2 and UiO-66.

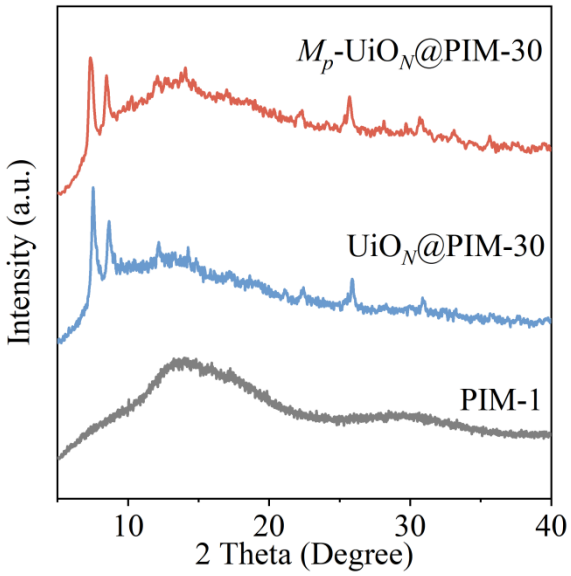

Fig. S4. XRD patterns of M_p-UiO$_N$@PIM-30 MMM, UiO$_N$@PIM-30 MMM, and PIM-1 membrane.

PIM-1 UiO_N@PIM-30 M_p-UiO_N@PIM-30

Fig. S5. Photographs of PIM-1 membrane, UiO_N@PIM-30 MMM, and M_p-UiO_N@PIM-30 MMM.

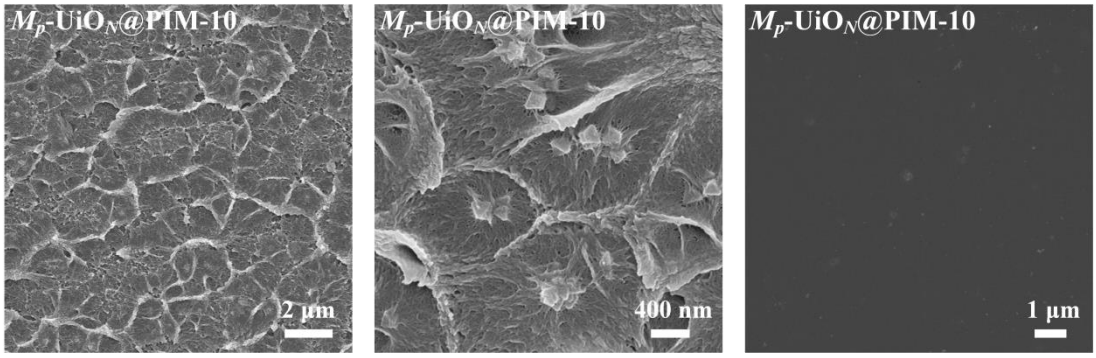

Fig. S6. SEM images of M_p-UiO$_N$@PIM-10 MMM.

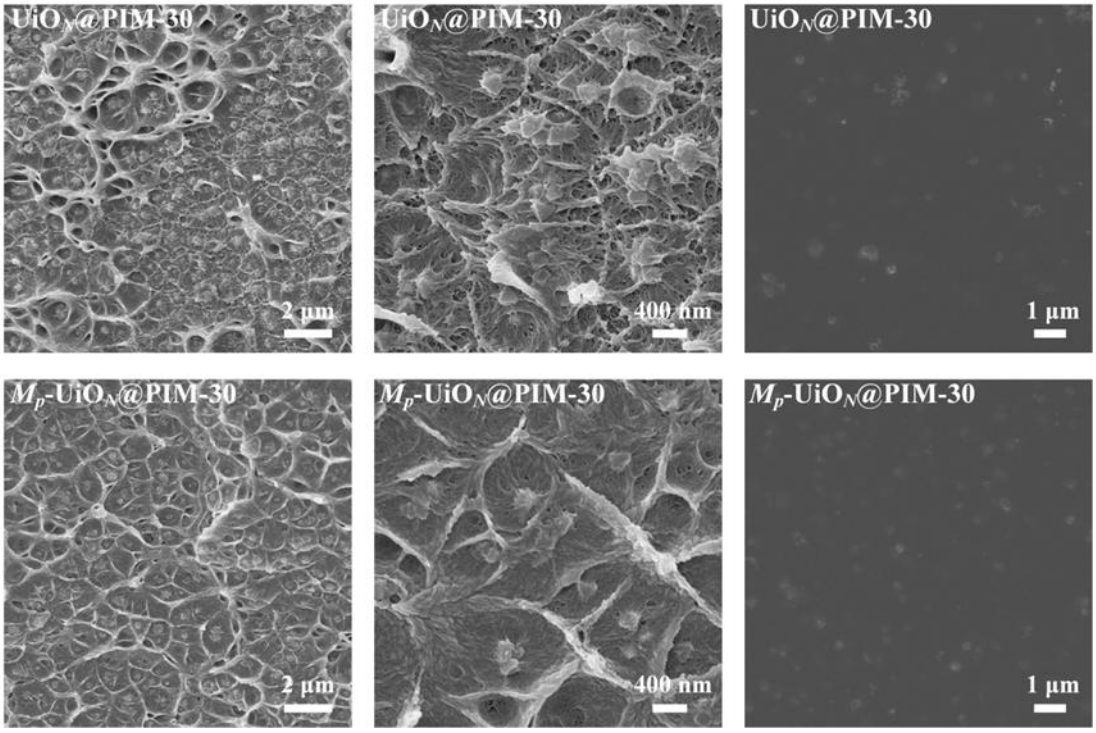

Fig. S7. SEM images of UiO$_N$@PIM-30 and M_p-UiO$_N$@PIM-30 MMMs.

More nanoparticles on the surface of M_p-UiO$_N$@PIM-30 MMM than that of UiO$_N$@PIM-30 MMM demonstrated the less sedimentation resulting from enhanced dispersity and compatibility.

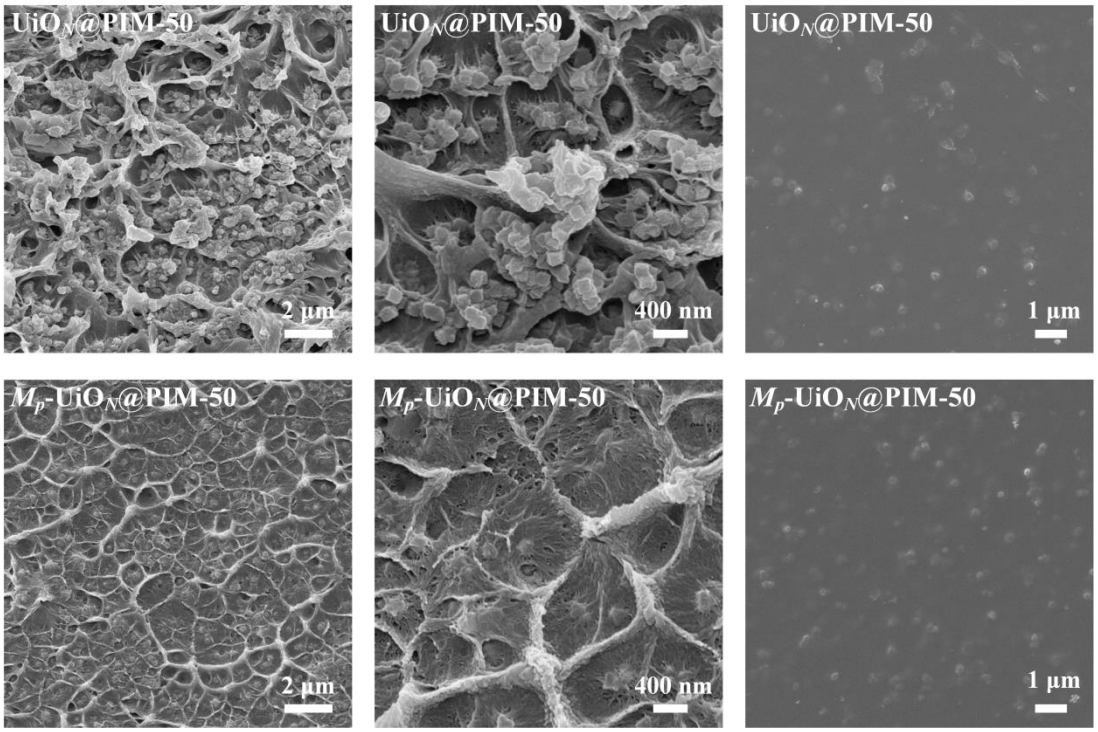

Fig. S8. SEM images of UiO$_N$@PIM-50 and M_p-UiO$_N$@PIM-50 MMMs.

More nanoparticles on the surface of M_p-UiO$_N$@PIM-50 MMM than that of UiO$_N$@PIM-50 MMM demonstrated the less sedimentation resulting from enhanced dispersity and compatibility.

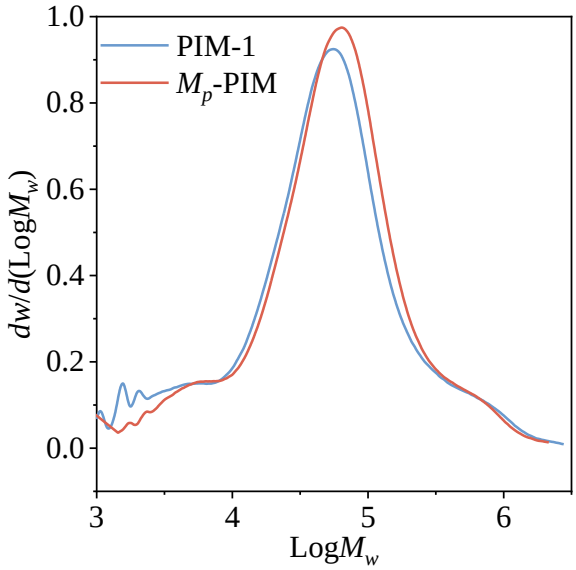

Fig. S9. Molecular weight distributions of PIM-1 and M_p-PIM.

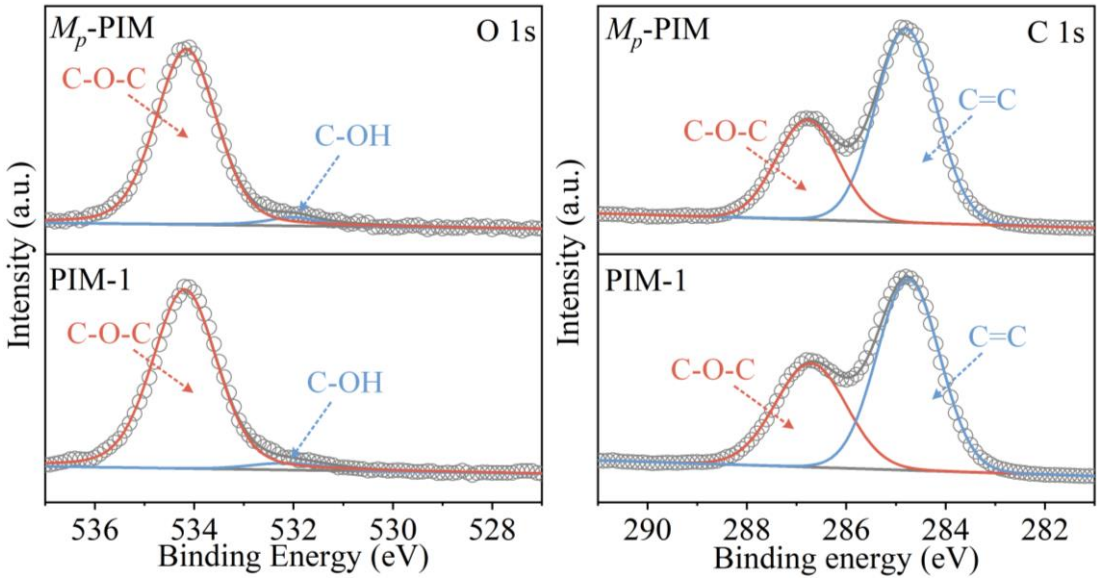

Fig. S10. High-resolution O 1s and C 1s XPS profiles of M_p-PIM and PIM-1.

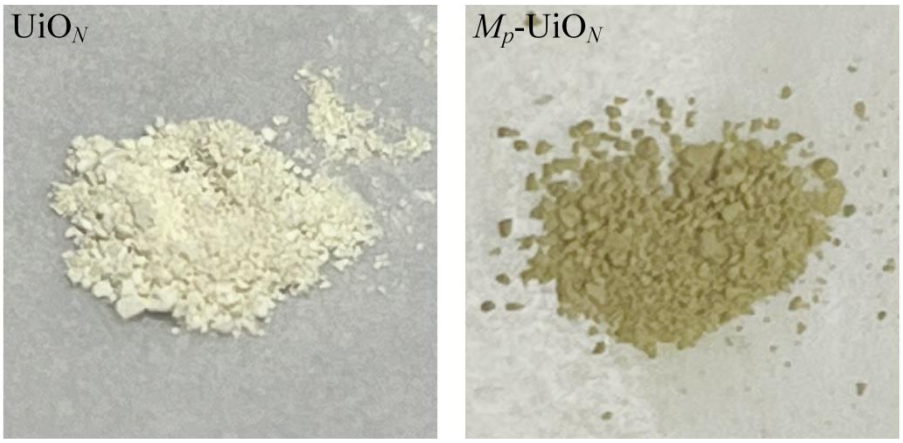

Fig. S11. Photographs of UiO$_N$ and M_p-UiO$_N$.

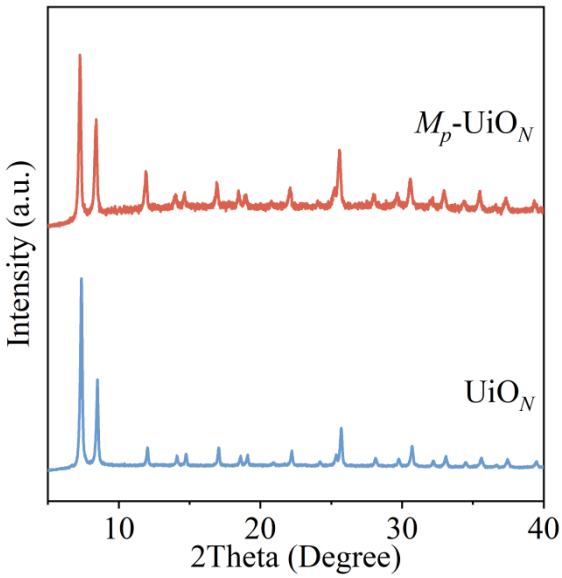

Fig. S12. XRD patterns of M_p-UiO$_N$ and UiO$_N$.

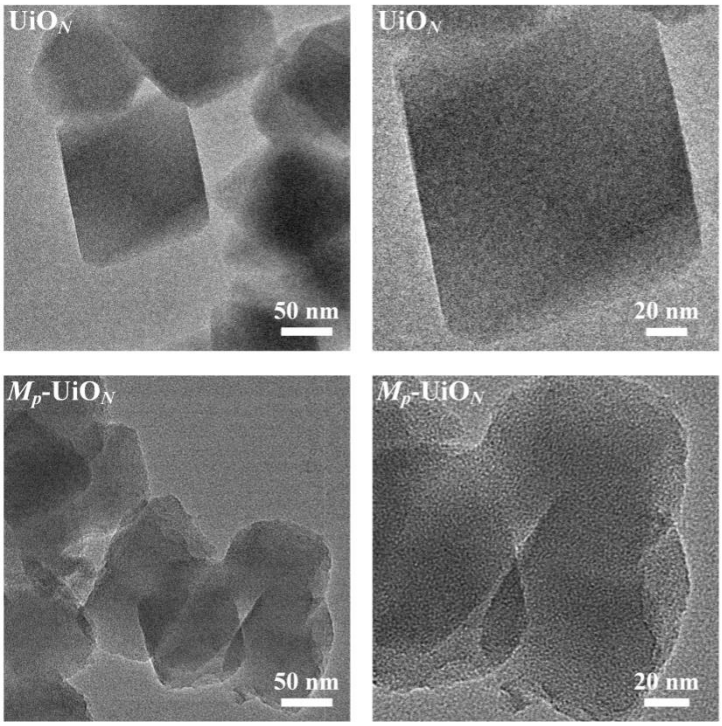

Fig. S13. TEM images of UiO$_N$ and M_p-UiO$_N$.

During ball milling, friction, shear, and impact forces promoted the deformation of fillers, in which case the polyhedral structure of UiO$_N$ was altered to near-spherical (M_p-UiO$_N$).

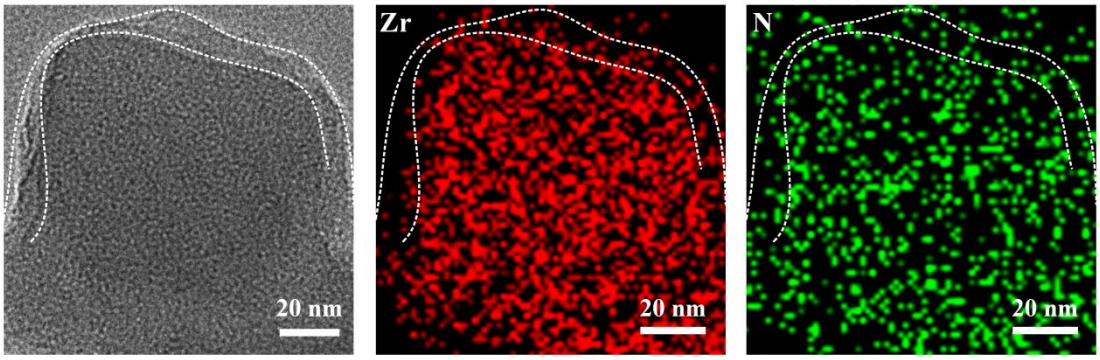

Fig. S14. Energy-dispersive spectroscopy mapping images of M_p-UiO$_N$.

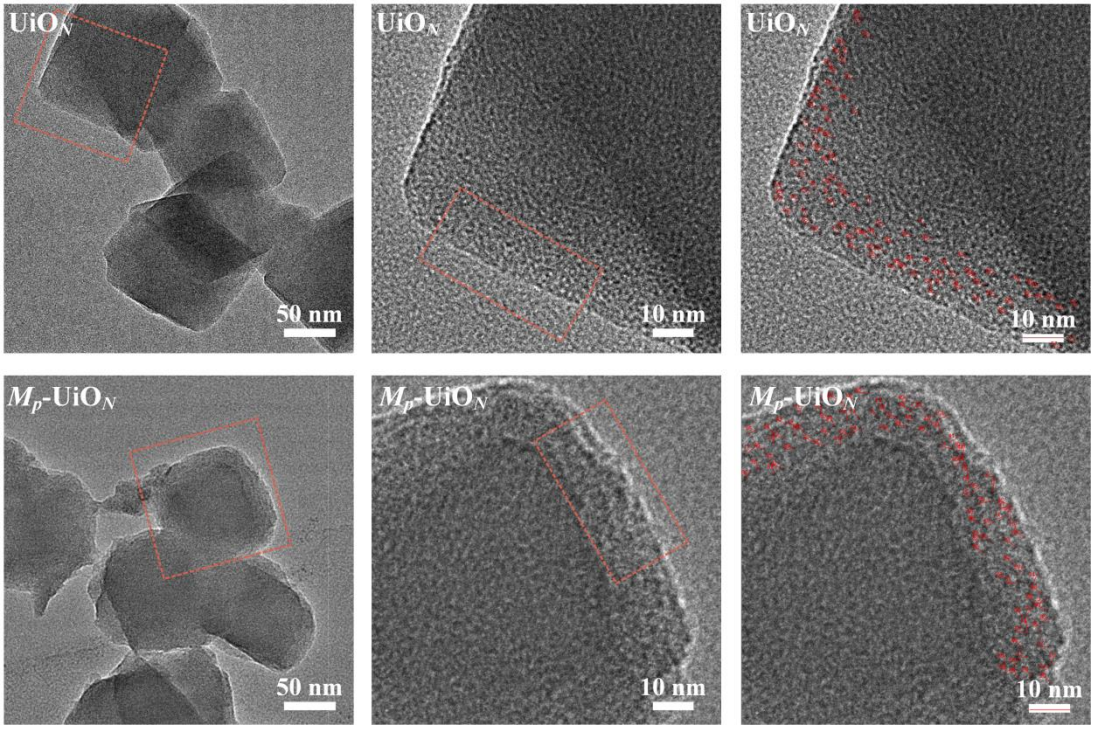

Fig. S15. Measurement for cluster-cluster distances of UiO$_N$ and M_p-UiO$_N$. Dash squares mark the regions mentioned in Fig. 2. Red lines represent distance measurement positions.

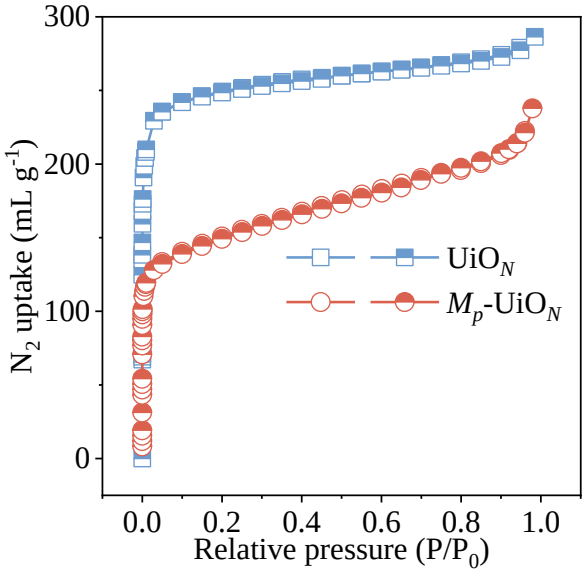

Fig. S16. Nitrogen adsorption-desorption isotherms of UiO_N and M_p-UiO_N at 77 K. Semi-solid and open symbols represent the adsorption and desorption branches, respectively.

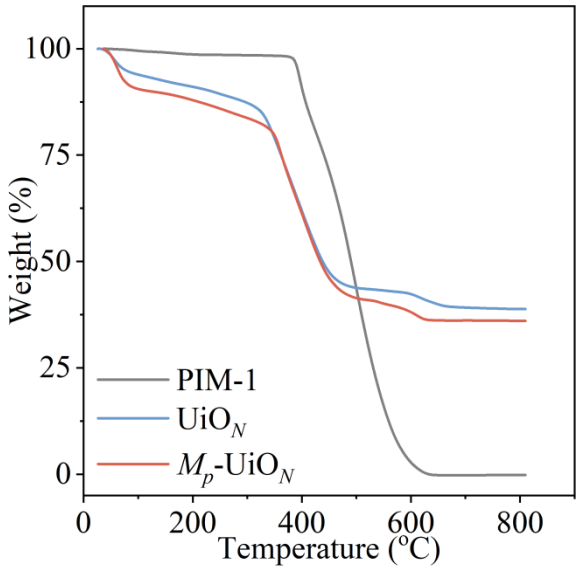

Fig. S17. Thermal gravimetric profiles of PIM-1, UiO$_N$, and M_p-UiO$_N$.

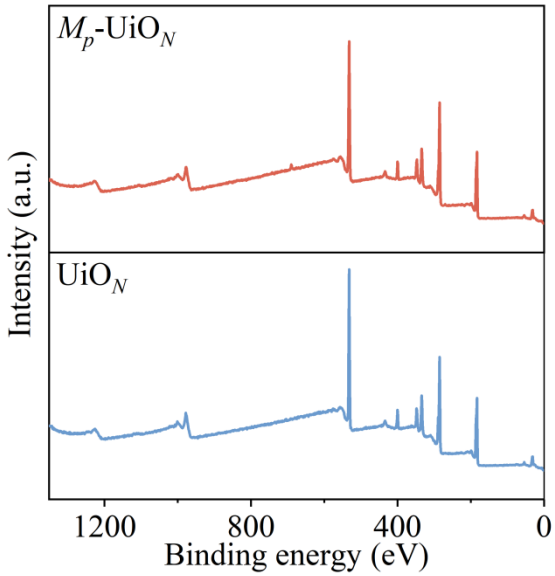

Fig. S18. Full XPS profiles of M_p-UiO$_N$ and UiO$_N$.

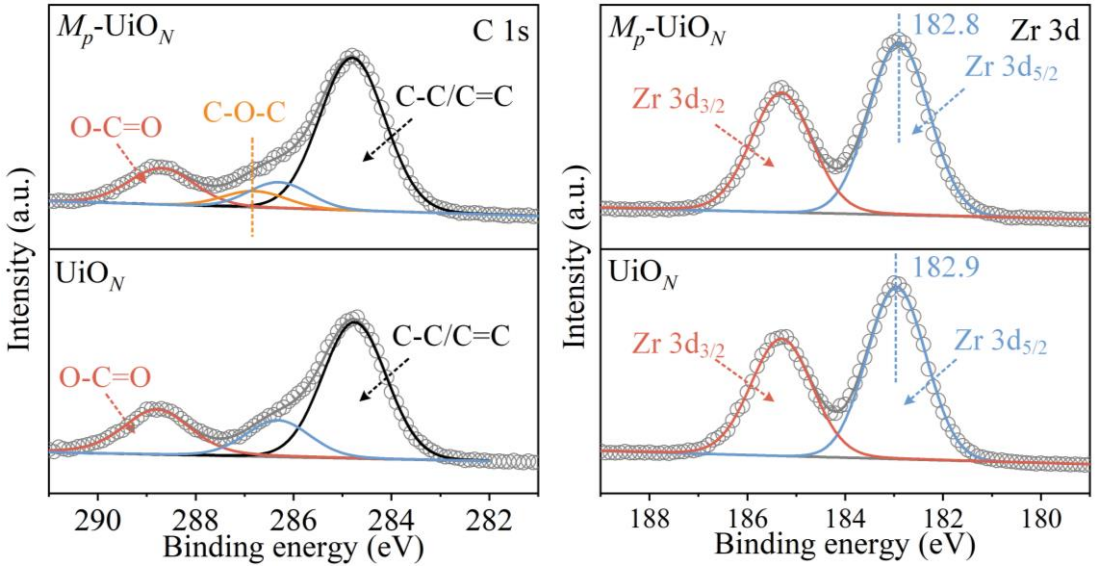

Fig. S19. High-resolution C 1s and Zr 3d XPS profiles of M_p-UiO$_N$ and UiO$_N$.

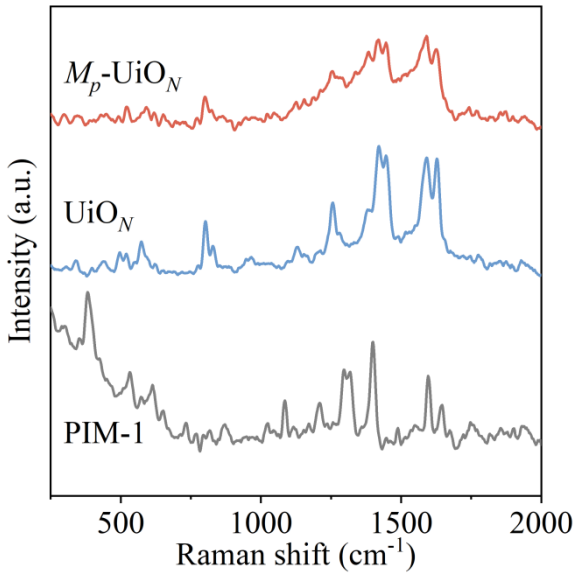

Fig. S20. Raman spectra of M_p-UiO$_N$, UiO$_N$, and PIM-1.

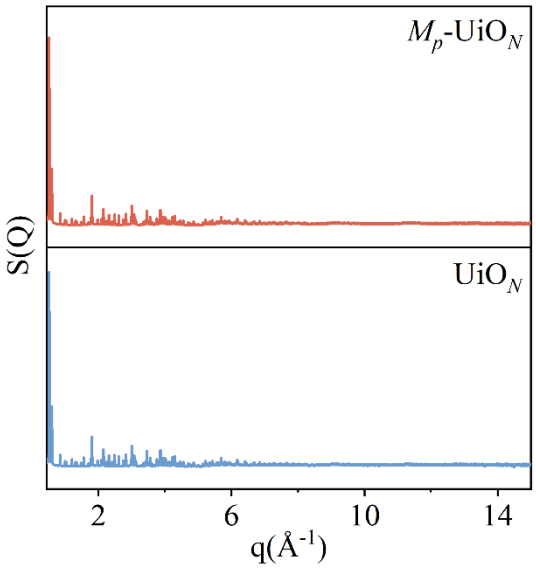

Fig. S21. X-ray total scattering data of M_p-UiO$_N$ and UiO$_N$.

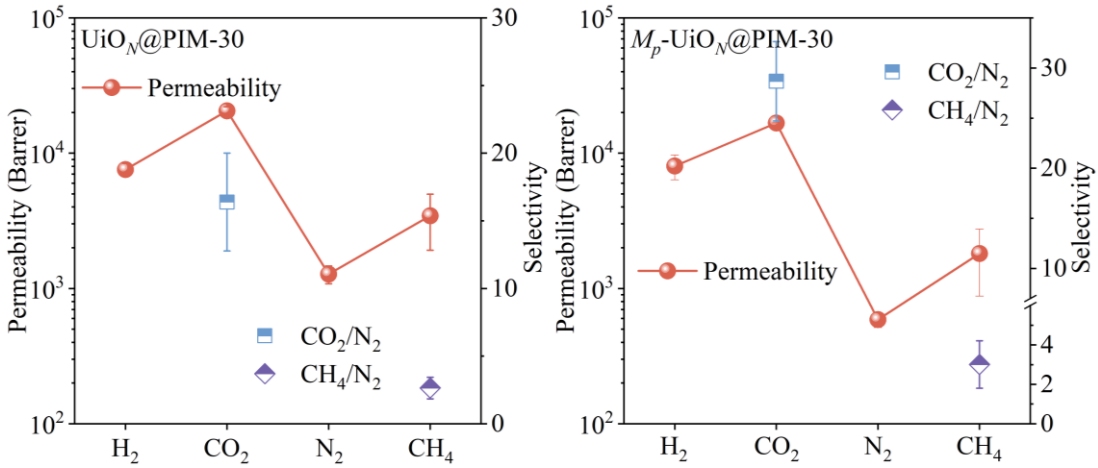

Fig. S22. Single-gas permeation behaviors of UiO$_N$@PIM-30 and M_p-UiO$_N$@PIM-30 MMMs.

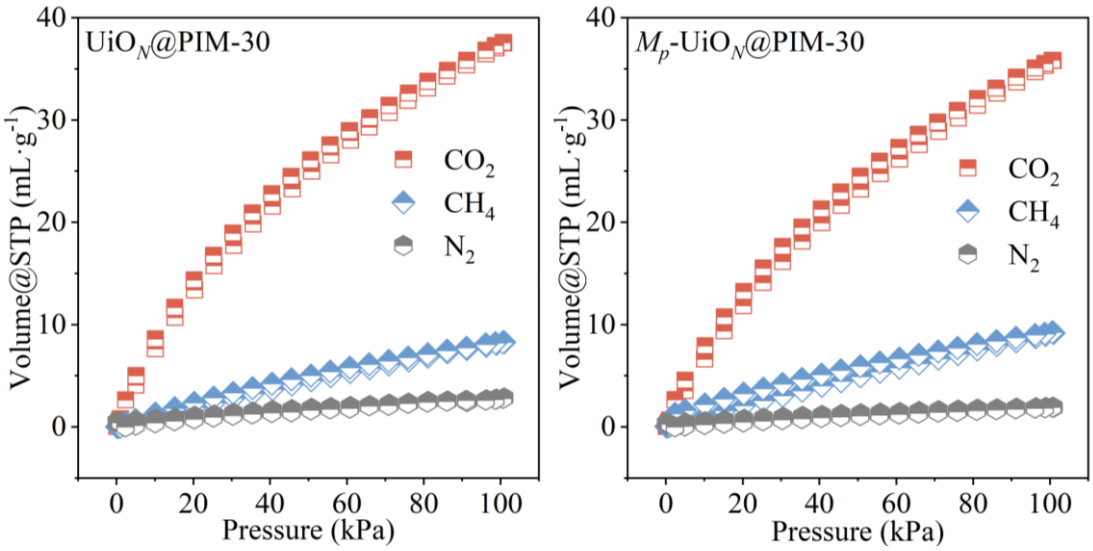

Fig. S23. Gas adsorption-desorption isotherms of UiO$_N$@PIM-30 and M_p-UiO$_N$@PIM-30 MMMs.

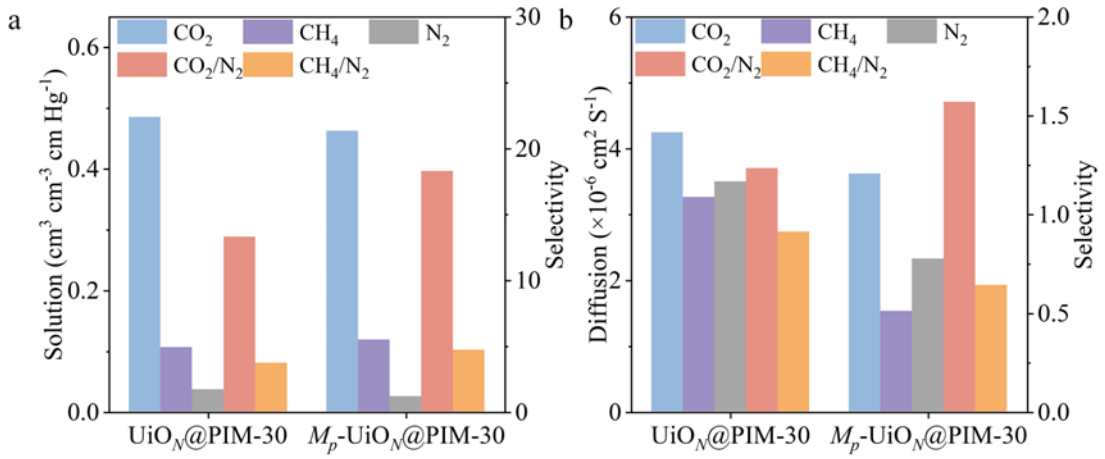

Fig. S24. Sorption and diffusion related coefficient and selectivity of M_p-UiO$_N$@PIM-30 and UiO$_N$@PIM-30 MMMs.

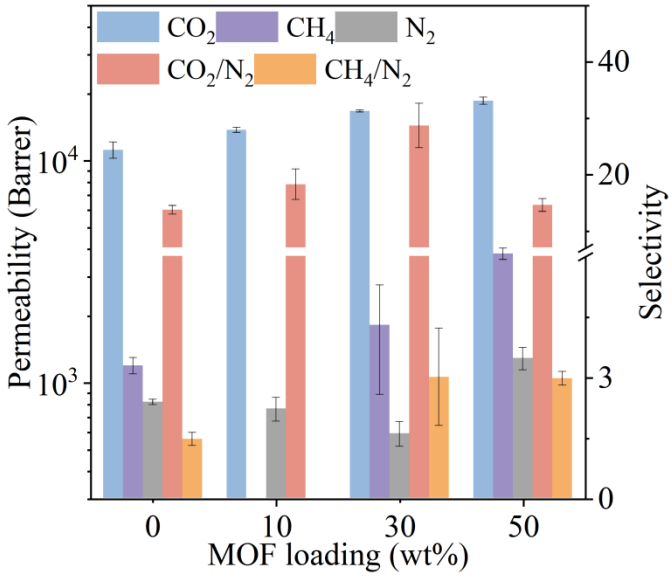

Fig. S25. Single-gas permeation behaviors of M_p-UiO$_N$@PIM MMMs with different loadings.

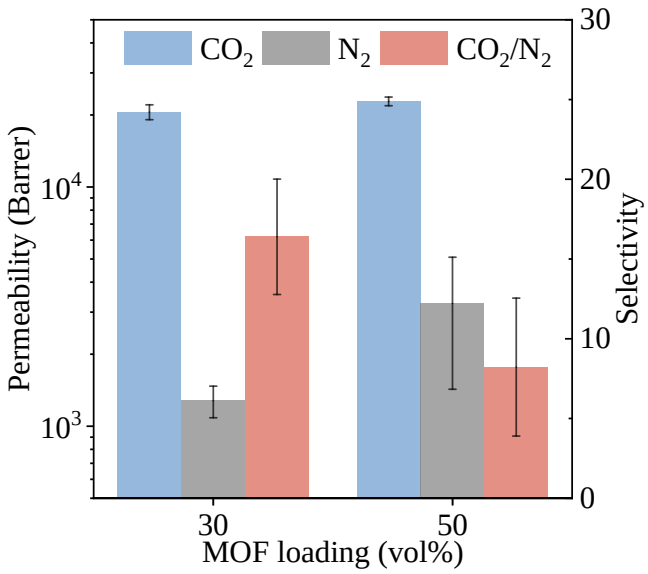

Fig. S26. Single-gas permeation behaviors of UiO_N@PIM MMMs with different loadings.

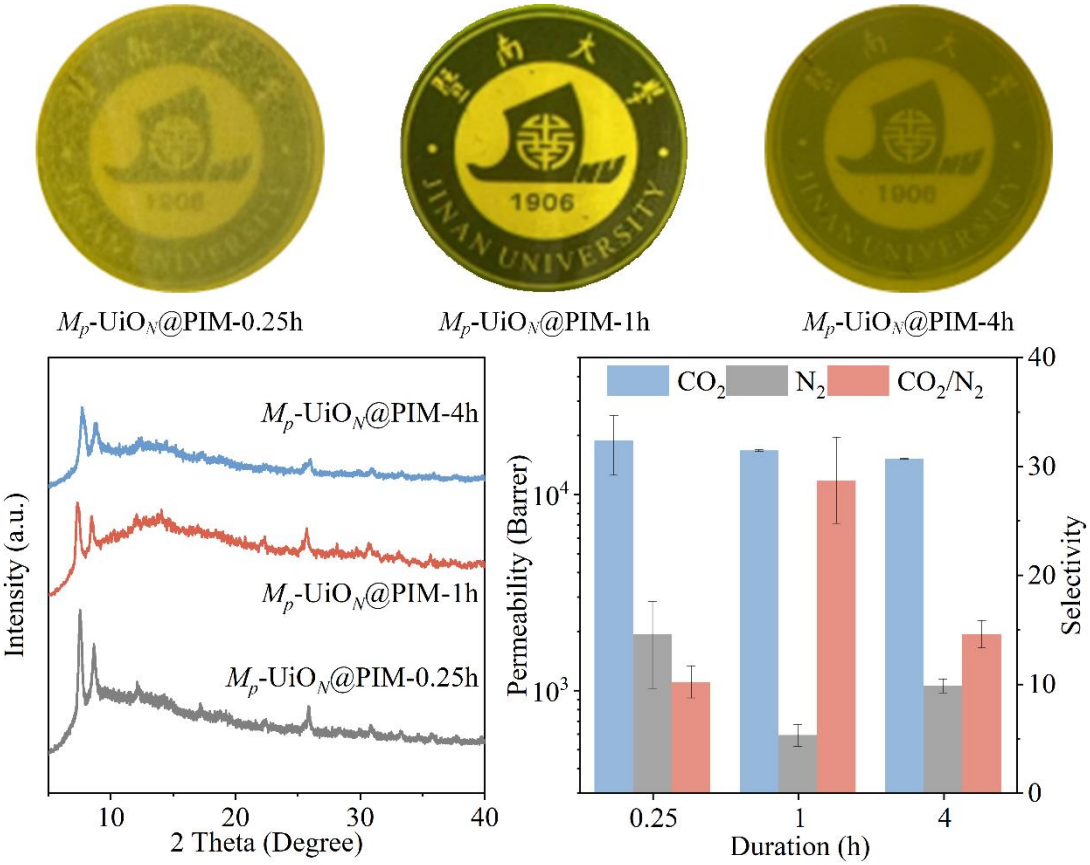

Fig. S27. Photographs, XRD patterns, and single-gas permeation behaviors of M_p-UiO$_N$@PIM MMMs with different ball milling durations.

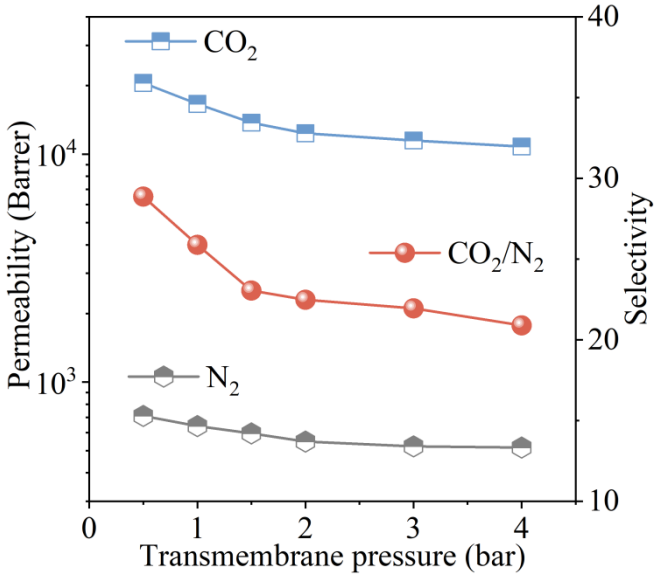

Fig. S28. Single-gas permeation behaviors of M_p-UiO$_N$@PIM-30 MMM at different transmembrane pressures.

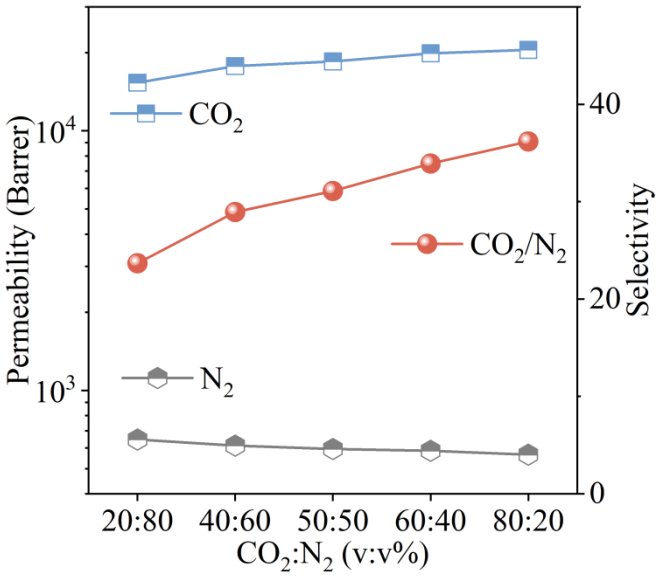

Fig. S29. Gas permeability and CO_2/N_2 selectivity of M_p-UiO$_N$@PIM-30 MMM after natural aging for 100 days for binary gas mixture with different CO_2 volume percentages.

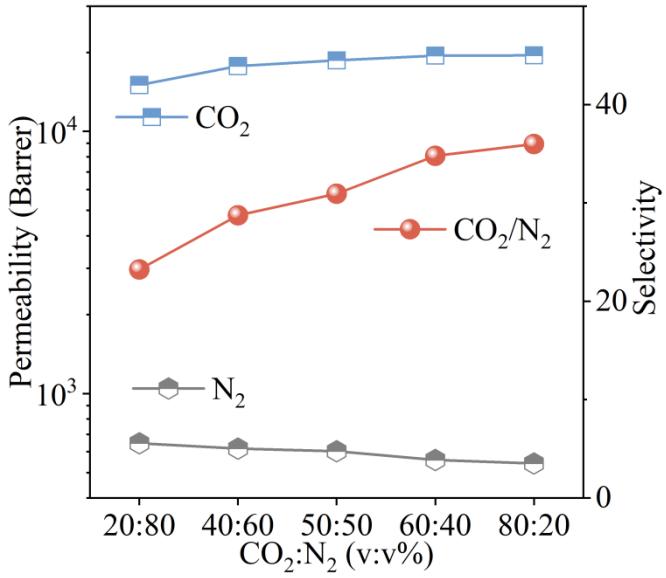

Fig. S30. Gas permeability and CO_2/N_2 selectivity of M_p-UiO$_N$@PIM-30 MMM after natural aging for 180 days for binary gas mixture with different CO_2 volume percentages.

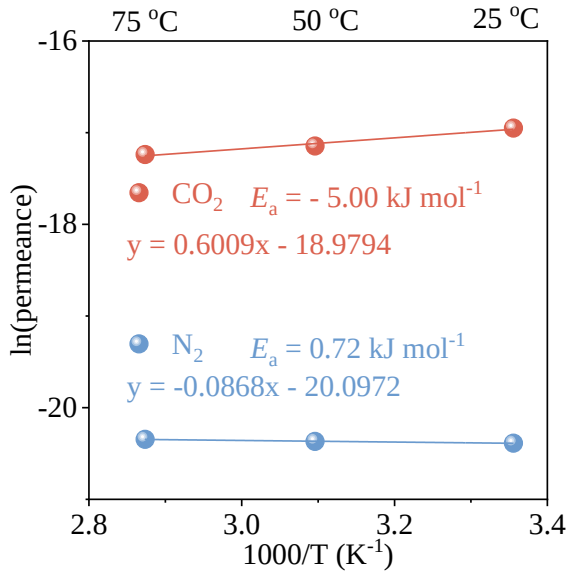

Fig. S31. Arrhenius temperature dependence of CO_2 and N_2 for M_p-UiO$_N$@PIM-30 MMM. A plot of ln(permeance) versus 1/T gives a straight line, whose slope is used to calculate activation energy (E_a). The unit of the permeance is mol m^{-2} s^{-1} Pa^{-1}. T is the absolute temperature (K) of mixed-gas separation.

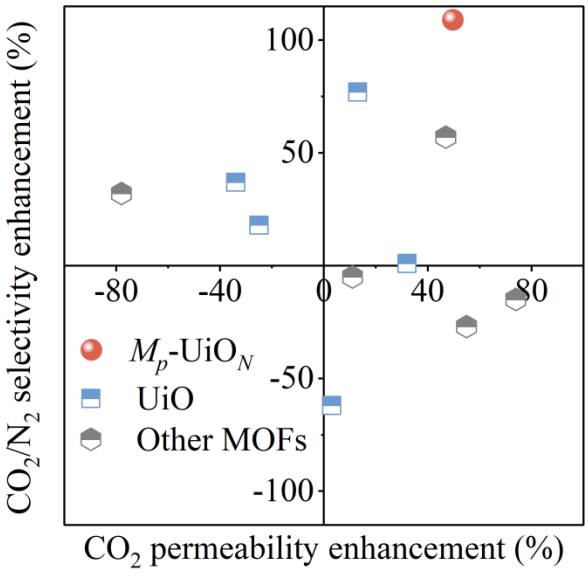

Fig. S32. Comparison of M_p-UiO$_N$@PIM-30 MMM in this study with other MOF@PIM MMMs for selectivity and permeability enhancements.

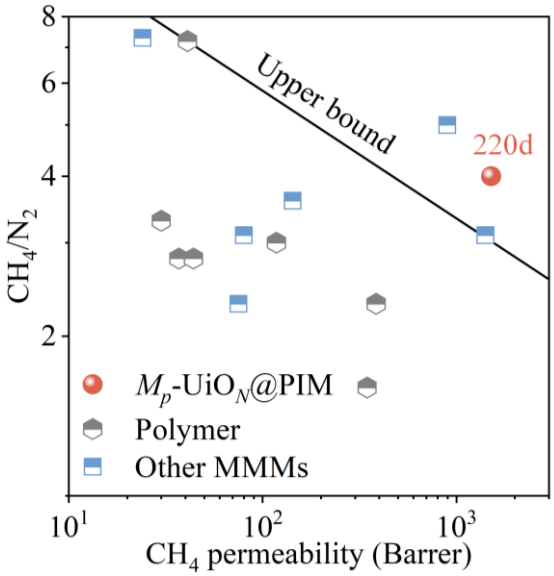

Fig. S33. Comparison of M_p-UiO$_N$@PIM-30 MMM in this study with other polymer membranes and MMMs for CH_4/N_2 separation.

PIM-1 UiO@PIM-30 M_p-UiO@PIM-30

Fig. S34. Photographs of PIM-1 membrane, UiO@PIM-30 MMM, and M_p-UiO@PIM-30 MMM.

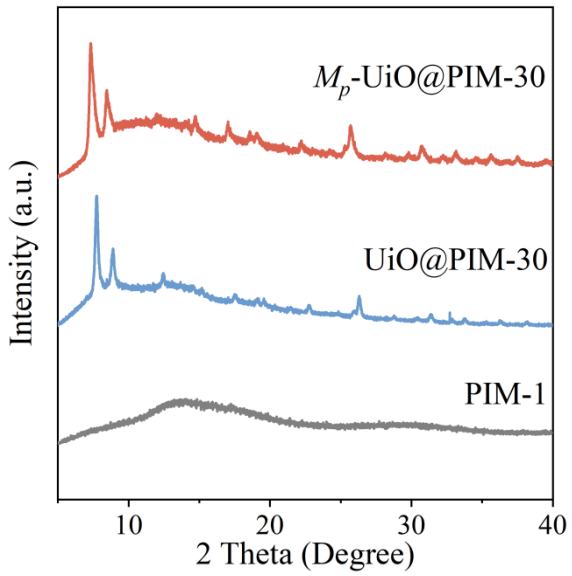

Fig. S35. XRD patterns of M_p-UiO@PIM-30 MMM, UiO@PIM-30 MMM, and PIM-1 membrane.

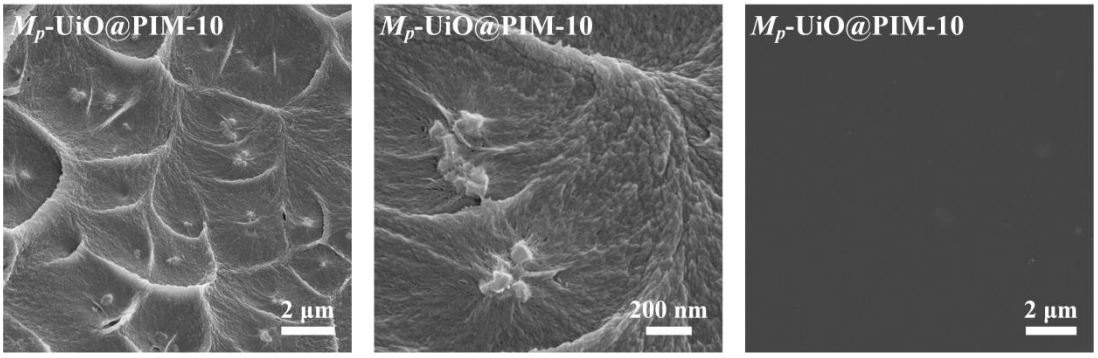

Fig. S36. SEM images of M_p-UiO@PIM-10 MMM.

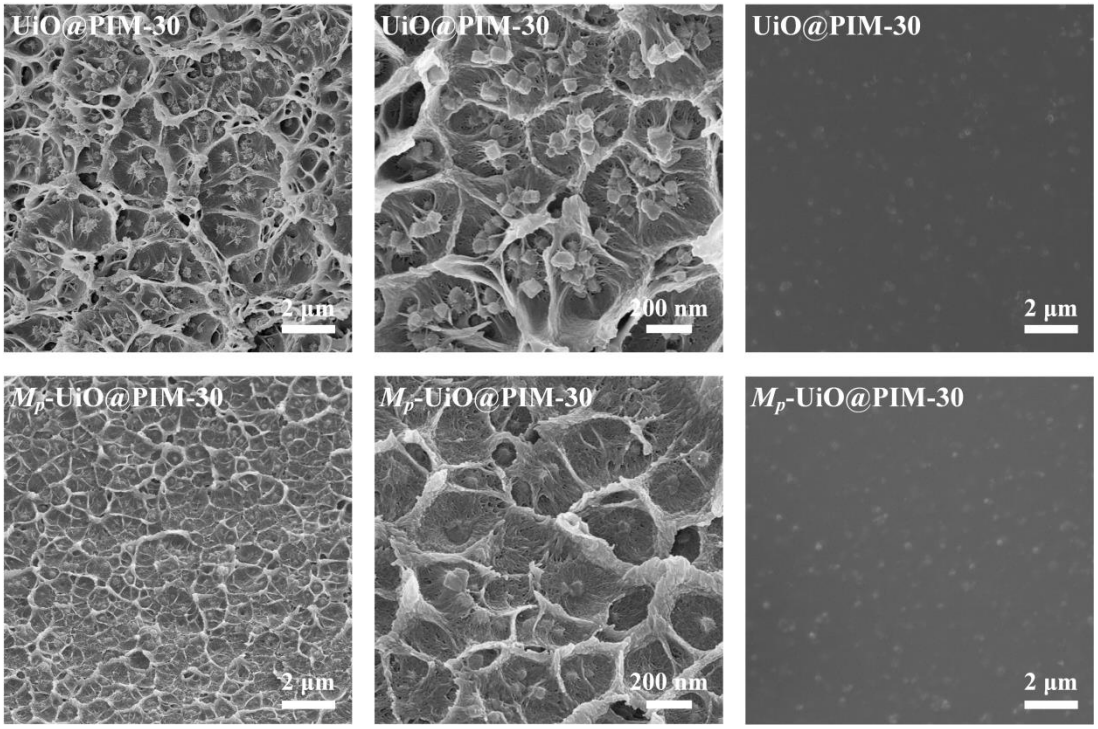

Fig. S37. SEM images of UiO@PIM-30 and M_p-UiO@PIM-30 MMMs.

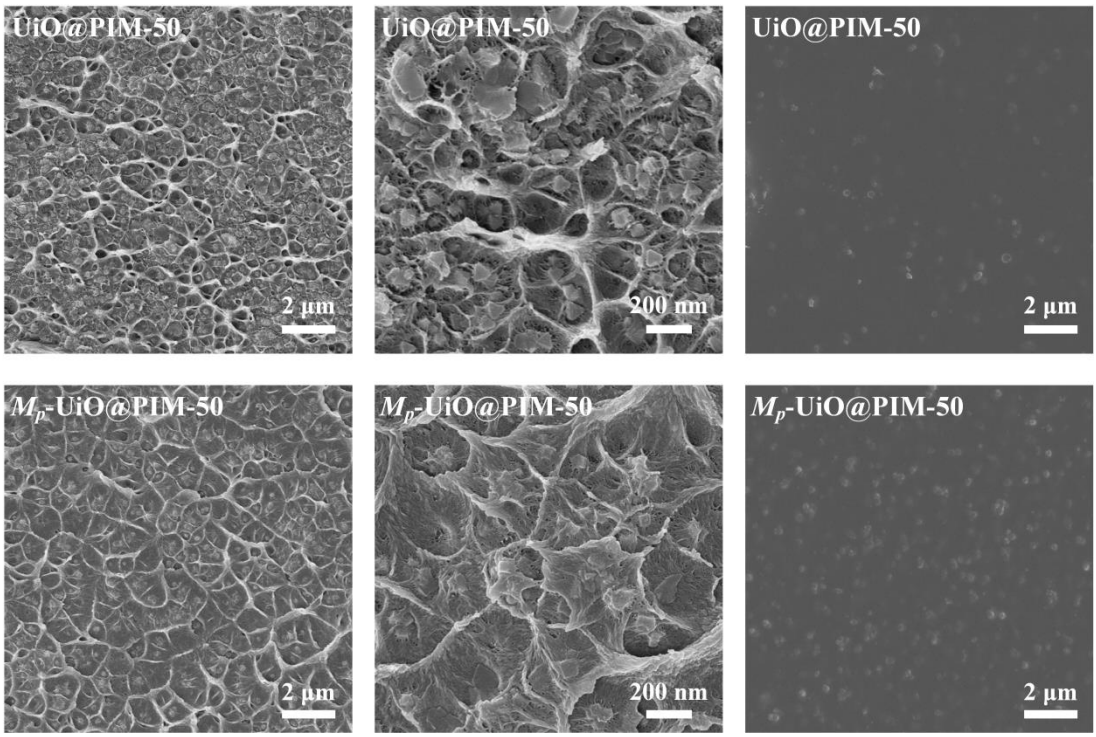

Fig. S38. SEM images of UiO@PIM-50 and M_p-UiO@PIM-50 MMMs.

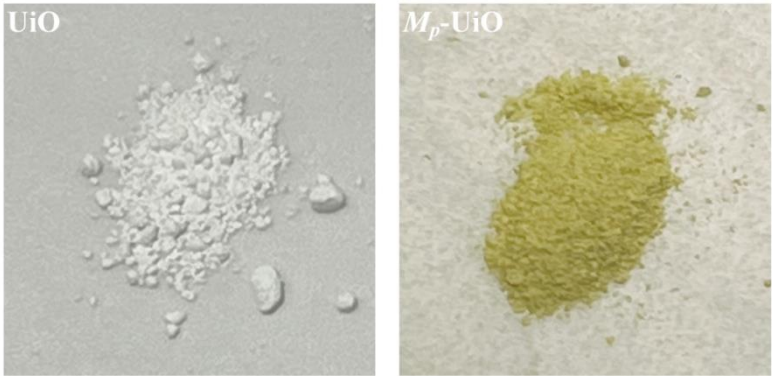

Fig. S39. Photographs of UiO and M_p-UiO.

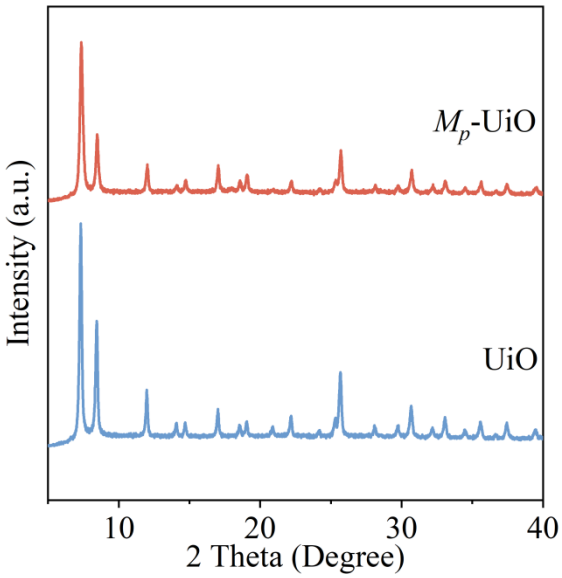

Fig. S40. Photographs of UiO and M_p-UiO.

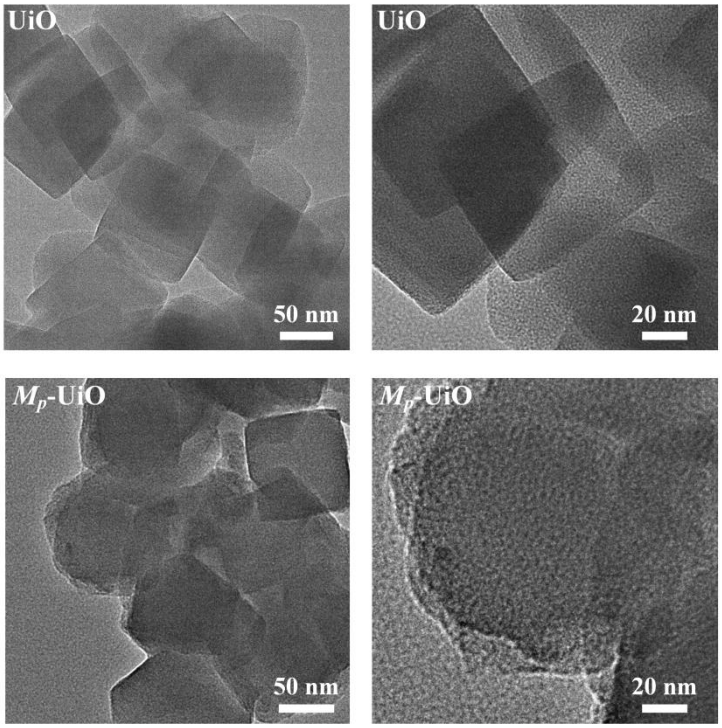

Fig. S41. TEM images of UiO and M_p-UiO.

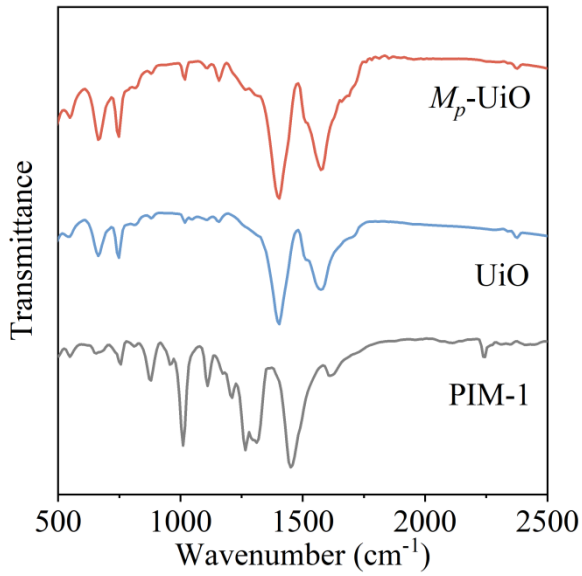

Fig. S42. FTIR spectra of M_p-UiO, UiO, and PIM-1.

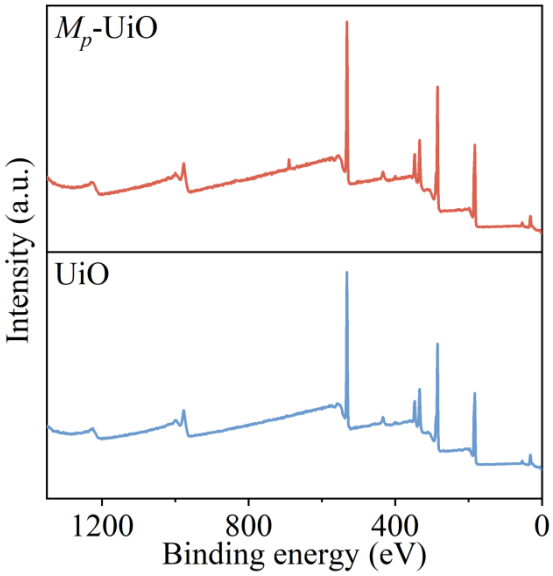

Fig. S43. Full XPS profiles of M_p-UiO and UiO.

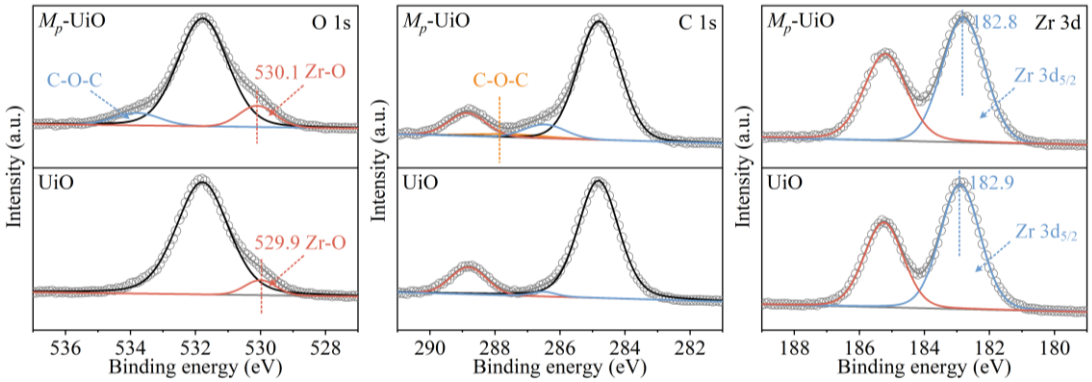

Fig. S44. High-resolution O 1s, C 1s, and Zr 3d XPS profiles of M_p-UiO and UiO.

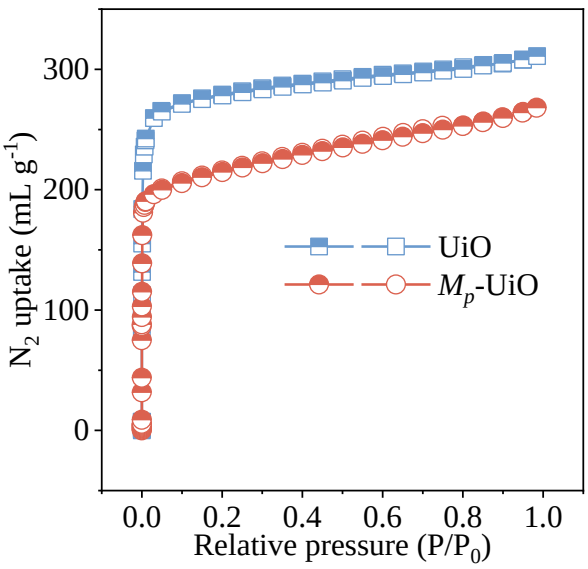

Fig. S45. Nitrogen adsorption-desorption isotherms of UiO and M_p-UiO at 77 K. Solid and open symbols represent the adsorption and desorption branches, respectively.

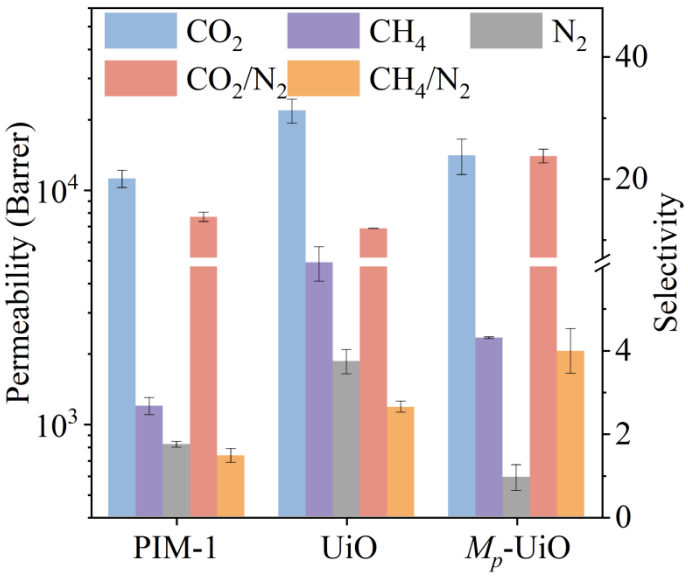

Fig. S46. Single-gas permeation behaviors of PIM-1 membrane, UiO@PIM-30 MMM, and M_p-UiO@PIM-30 MMM.

Table S1. Interaction energies of PIM-1 with different UiO_N.

UiO_N	Average interaction energy (kJ mol^{-1})
Bidentate	-5.11
Monodentate	-7.26
Disconnected	-10.40

Table S2. Single-gas permeation behaviors of M_p-UiO$_N$@PIM and UiO$_N$@PIM MMMs with different loadings.

Membranes	Permeability (Barrer)			Selectivity	
	CO_2	CH_4	N_2	CO_2/N_2	CH_4/N_2
PIM-1	11165 ±947	1189 ±100	814 ±23	13.7 ±0.8	1.5 ±0.2
UiO$_N$@PIM-30	20575 ±1470	/	1277 ±193	16.4 ±3.6	/
UiO$_N$@PIM-50	22815 ±956	/	3257 ±1830	8.2 ±4.3	/
M_p-UiO$_N$@PIM-10	13727 ±368	/	760 ±93	18.2 ±2.7	/
M_p-UiO$_N$@PIM-30	16721 ±177	2082 ±346	584 ±82	28.6 ±4.0	3.6 ±0.3
M_p-UiO$_N$@PIM-50	18591 ±700	3800 ±224	1284 ±148	14.6 ±1.1	3.0 ±0.2

Table S3. Performance summary of polymer membranes and MMMs for CO_2/N_2 separation. PD-polydopamine; PI-polyimide; PEO-polyethylene oxide and MEEP100-[2-(2-methoxyethoxy)ethoxy] polyphosphazene.

Membranes	Permeability (Barrer)	CO_2/N_2 selectivity	Temp (^oC)	Gas types	Ref.
UiO-66-Br/PIM-1	2294	19.0	25	Single	4
UiO-66-NH_2/PIM-1	2005	22.0	25	Single	4
ZIF-8/PIM-1	13564	16.5	35	Single	5
HZIF-8/PIM-1	8268	25.1	35	Single	5
PhUiO-66/PIM-1	9040	23.2	25	Single	6
UiO-66-CN/sPIM-1	10354	33.2	25	Mixed (15:85)	7
UiO-66-NH_2/sPIM-1	8620	18.0	25	Single	7
ZIF-8/Polyimide	783	18.0	35	Mixed (50:50)	8
ZIF-8/PD-PI	695	21.0	35	Mixed (50:50)	8
NUS-8-NH_2/PIM-1	14638	29.2	25	Mixed (20:80)	9
MOF-801/PIM-1	9686	27.0	35	Single	10
MOF-303/PIM-1	6199	22.1	35	Mixed (20:80)	11
MUF-15-NS/PIM-1	13180	19.6	20	Mixed (50:50)	12
MIL-101/PIM-1	22000	15.4	25	Single	13
NanoMIL-101/PIM-1	10600	19.3	25	Single	13
NUS-8/PIM-1	6725	26.8	25	Mixed (50:50)	14

NUS-8-COOH/PIM-1	11512	31.0	25	Mixed (50:50)	15
UiO-66-NH_2/AO-PIM-1	9420	15.6	35	Single	16
ZIF-67/PIM-1	5206	24.2	30	Single	17
ZIF-8/PIM-1	6820	17.9	20	Single	18
ZIF-8/PEO	2490	37.0	35	Single	19
UiO-66-NH_2/PIM-PI-1	3895	13.4	30	Single	20
PPM-10/PIM-PI-1	3827	24.0	30	Single	20
ZIF-8/PIM-1	6338	24.4	35	Single	21
ZIF-8/PIM-1	6242	23.4	35	Mixed (20:80)	21
UiO-66-NH_2/PIM-1	6310	22.0	25	Single	22
UiO-66/PIM-1	4940	13.6	25	Single	22
UiO-66-NH_2/PIM-1	6419	26.0	35	Single	23
UiO-66/AO-PIM-1	1380	27.0	35	Single	24
AO-PIM-1	986	29.8	35	Single	24
PIM-1	5135	14.4	22	Single	25
TOX-PIM-1	1100	37.0	22	Single	25
PIM-1	12600	25.5	23	Single	26
PIM-1	13600	16.5	25	Single	27
PIM-1	11430	17.5	-	Single	28
PIM-1	11840	18.2	20	Single	29

PIM-1	12355	19.8	25	Single	30
PIM-1	9968	15.9	27	Mixed (15:85)	31
MEEP100/PIM-1	5340	24.0	22	Mixed (50:50)	32

Table S4. Performance summary of MOF@PIM-1 MMMs for CO_2/N_2 separation. PE-permeability enhancement and SE-selectivity enhancement.

MOFs	Permeability (Barrer)	CO_2/N_2 selectivity	PE (%)	SE (%)	Ref.
UiO-66-Br	2294	19.0	-25	18	4
UiO-66-NH_2	2005	22.0	-34	37	4
PhUiO-66	9040	23.2	13	77	6
MOF-801	4660	19.0	11	-5	10
ZIF-8	6820	17.9	55	-27	13
UiO-66	4940	13.6	3	-62	22
UiO-66-NH_2	6310	22.0	32	1	22
ZIF-8	11975	14.0	74	-15	33
ZIF-B	10079	25.9	47	57	33
UiO-66	5378	26.6	65	10	34
UiO-66-$(CF_3)_2$	5242	33.8	61	40	34
ZIF-8	1365	25.1	-78	32	35

Table S5. Performance summary of polymer membranes and MMMs for CH_4/N_2 separation. PAA-polyacrylic acid; SBS-poly (styrene-b-butadiene-b-styrene); Pebax-poly(ether-b-amide); EVA-ethylene vinyl acetate and PMHS-poly(methylhydrosiloxane).

Membranes	Permeability (Barrer)	CH_4/N_2 selectivity	Temp (^oC)	Gas types	Ref.
ZIF-8/PIM-A	897	5.0	25	Mixed (50:50)	36
PIM-A	346	1.6	25	Single	36
ZIF-8@VR-800/PAA	1410	3.1	25	Single	37
Ni-MOF-74/SBS-15	75	2.3	25	Mixed (50:50)	38
SBS	37	2.8	25	Mixed (50:50)	38
Pebax/EVA	385	2.3	55	Single	39
SBS	41	7.2	25	Single	40
Pebax/SBS	44	2.8	25	Single	41
Pebax2533	30	3.3	25	Single	41
SBS-c-PMHS	118	3.0	25	Single	42
$[Ni_3(HCOO)_6]$/SBS-5	80	3.1	25	Single	43
SBS10SN	24	7.3	25	Single	44
ZIF-8/Pebax-2533	143	3.6	25	Single	45

References

1. A. K. Rappe, C. J. Casewit, K. S. Colwell, W. A. Goddard, W. M. Skiff, UFF, *J. Am. Chem. Soc.*, 1992, **114**, 10024.
2. E. S. Kadantsev, P. G. Boyd, T. D. Daff, T. K. Woo, *J. Phys. Chem. Lett.*, 2013, **4**, 3056–3061.
3. W. D. Cornell, P. Cieplak, C. I. Bayly, I. R. Gould, K. M. Merz, D. M. Ferguson, D. C. Spellmeyer, T. Fox, J. W. Caldwell, P. A. Kollman, *J. Am. Chem. Soc.*, 1995, **117**, 5179–5197.
4. B. Ghalei, K. Sakurai, Y. Kinoshita, K. Wakimoto, A. P. Isfahani, Q. Song, K. Doitomi, S. Furukawa, H. Hirao, H. Kusuda, S. Kitagawa, E. Sivaniah, *Nat. Energy*, 2017, **2**, 17086.
5. B. Zhu, S. He, Y. Yang, S. Li, C. H. Lau, S. Liu, L. Shao, *Nat. Commun.*, 2023, **14**, 1697.
6. P. Su, S. Chen, L. Chen, W. Li, *J. Membr. Sci.*, 2024, **691**, 122246.
7. G. Yu, X. Zou, L. Sun, B. Liu, Z. Wang, P. Zhang, G. Zhu, *Adv. Mater.*, 2019, **31**, 1806853.
8. Z. Wang, D. Wang, S. Zhang, L. Hu, J. Jin, *Adv. Mater.*, 2016, **28**, 3399–3405.
9. Y. Pu, Z. Yang, V. Wee, Z. Wu, Z. Jiang, D. Zhao, *J. Membr. Sci.*, 2022, **641**, 119912.
10. W. Chen, Z. Zhang, L. Hou, C. Yang, H. Shen, K. Yang, Z. Wang, *Sep. Purif. Technol.*, 2020, **250**, 117198.
11. Q. Shen, S. Cong, H. Zhu, Y. Zhang, R. He, S. Yi, Y. Zhang, *J. Membr. Sci.*, 2022, **664**, 121107.
12. H. Yin, A. Alkaş¸, Y. Zhang, Y. Zhang, S. G. Telfer, *J. Membr. Sci.*, 2020, **609**, 118245.
13. M. Khdhayyer, A. F. Bushell, P. M. Budd, M. P. Attfield, D. Jiang, A. D. Burrows, E. Esposito, P. Bernardo, M. Monteleone, A. Fuoco, G. Clarizia, F. Bazzarelli, A. Gordano, J. C. Jansen, *Sep. Purif. Technol.*, 2019, **212**, 545–554.

14. Y. Cheng, S. R. Tavares, C. M. Doherty, Y. Ying, E. Sarnello, G. Maurin, M. R. Hill, T. Li, D. Zhao, *ACS Appl. Mater. Interfaces*, 2018, **10**, 43095−43103.
15. D. Wang, Y. Ying, Y. Zhang, Y. Pu, Z. Yang, D. Zhao, *J. Membr. Sci.*, 2022, **2**, 100017.
16. Z. Wang, H. Ren, S. Zhang, F. Zhang, J. Jin, *J. Mater. Chem. A*, 2017, **5**, 10968.
17. X. Wu, W. Liu, H. Wu, X. Zong, L. Yang, Y. Wu, Y. Ren, C. Shi, S. Wang, Z. Jiang, *J. Membr. Sci.*, 2018, **548**, 309−318.
18. A. F. Bushell, M. P. Attfield, C. R. Mason, P. M. Budd, Y. Yampolskii, L. Starannikova, A. Rebrov, F. Bazzarelli, P. Bernardo, J. C. Jansen, M. Lanč, K. Friess, V. Shantarovich, V. Gustov, V. Isaeva, *J. Membr. Sci.*, 2013, **427**, 48−62.
19. S. Li, Y. Sun, Z. Wang, C. Jin, M. Yin, Q. An, *Small*, 2023, **19**, 2208177.
20. A. Husna, I. Hossain, O. Choi, S. M. Lee, T. H. Kim, Efficient CO_2 separation using a PIM-PI-functionalized UiO-66 MOF incorporated mixed matrix membrane in a PIM-PI-1 polymer, *Macromol. Mater. Eng.*, 2021, **306**, 2100298.
21. S. He, B. Zhu, X. Jiang, G. Han, S. Li, C. H. Lau, Y. Wu, Y. Zhang, L. Shao, *Proc. Natl. Acad. Sci. U. S. A.*, 2022, **119**, e2114964119.
22. M. R. Khdhayyer, E. Esposito, A. Fuoco, M. Monteleone, L. Giorno, J. C. Jansen, M. P. Attfield, P. M. Budd, *Sep. Purif. Technol.*, 2017, **173**, 304−313.
23. M. Liu, M. D. Nothling, P. A. Webley, J. Jin, Q. Fu, G. G. Qiao, *Chem. Eng. J.*, 2020, **396**, 125328.
24. I. D. Carja, S. R. Tavares, O. Shekhah, A. Ozcan, R. Semino, V. S. Kale, M. Eddaoud, G. Maurin, *ACS Appl. Mater. Interfaces*, 2021, **13**, 29041−29047.
25. Q. Song, S. Cao, R. H. Pritchard, B. Ghalei, S. A. Al-Muhtaseb, E. M. Tarentjev, A. K. Cheetham, E. Sivaniah, *Nat. Commun.*, 2014, **5**, 4813.
26. P. M. Budd, N. B. McKeown, B. S. Ghanem, K. J. Msayib, D. Fritsch, L. Starannikova, N. Belov, O. Sanfirova, Y. Yampolskii, V. Shantarovich, *J. Membr. Sci.*, 2008, **325**, 851-

860.

27. C. G. Bezzu, M. Carta, A. Tonkins, J. C. Jansen, P. Bernardo, F. Bazzarelli, N. B. McKeown, *Adv. Mater.* 2012, **24**, 5930-5933.
28. R. Hou, S. J. D. Smith, C. D. Wood, R. J. Mulder, C. H. Lau, H. Wang, M. R. Hill, *ACS Appl. Mater. Interfaces*, 2019, **11**, 6502-6511.
29. H. Yin, A. Alkaş, Y. Zhang, Y. Zhang, S. G. Telfer, *J. Membr. Sci.*, 2020, **609**, 118245.
30. R. Hou, S. J. D. Smith, K. Konstas, C. M. Doherty, C. D. Easton, J. Park, H. Yoon, H. Wang, B. D. Freeman, M. R. Hill, *J. Mater. Chem. A*, 2022, **10**, 10107-10119.
31. Z. Tian, D. Li, W. Zheng, Q. Chang, Y. Sang, F. Lai, J. Wang, Y. Zhang, T. Liu, M. Antonietti, *Mater. Horiz.*, 2023, **10**, 3660-3667.
32. A. K. Sekizkardes, S. Budhathoki, L. Zhu, V. Kusuma, Z. Tong, J. S. McNally, J. A. Steckel, S. Yi, D. Hopkinson, *J. Membr. Sci.*, 2021, **640**, 119764.
33. J. Huang, H. Tang, X. Huang, Z. Feng, P. Su, W. Li, *J. Membr. Sci.*, 2023, **668**, 121238.
34. Z. Zhou, X. Cao, D. Lv, F. Cheng, *Sep. Purif. Technol.*, 2024, **339**, 126666.
35. A. Fuoco, M. R. Khdhayyer, M. P. Attfield, E. Esposito, J. C. Jansen, P. M. Budd, *Membranes*, 2017, **7**, 7.
36. X. Huang, L. Chen, S. Chen, P. Su, W. Li, *J. Membr. Sci.* 2023, **685**, 121984.
37. Z. Gu, Z. Yang, X. Guo, Z. Qiao, C. Zhong, *Sep. Purif. Technol.*, 2021, **272**, 118845.
38. S. Wang, Q. Guo, S. Liang, P. Li, J. Luo, *Sep. Purif. Technol.*, 2018, **199**, 206−213.
39. Q. Xin, Y. Pan, C. Zhang, L. Zhang, C. Dong, L. Lin, L. Zhao, H. Ye, Y. Zhang, *Sep. Purif. Technol.*, 2024, **336**, 126302.
40. M. G. Buonomenna, G. Golemme, C. M. Tone, M. P. De Santo, F. Ciuchi, E. Perrotta, *Adv. Funct. Mater.*, 2012, **22**, 1759–1767.
41. P. Guan, J. Luo, W. Li, Z. Si, *Macromol. Res.*, 2017, **25**, 1007–1014.
42. J. Luo, T. Zhu, Y. Song, Z. Si, *Polymer*, 2017, **127**, 52–65.

43. S. Wang, Q. Guo, S. Liang, P. Li, X. Li, J. Luo, *Chem. Eng. Technol.*, 2018, **41**, 353–366.

44. M. G. Buonomenna, G. Golemme, C. M. Tone, M. P. De Santo, F. Ciuchi, E. Perrotta, *J. Mater. Chem. A*, 2013, **1**, 11853.

45. V. Nafisi, M. B. Hägg, *J. Membr. Sci.*, 2014, **459**, 244–255.